Author Manuscript
Accepted for publication in a peer-reviewed journal

NIST National Institute of Standards and Technology • U.S. Department of Commerce

Published in final edited form as:
DNA Repair (Amst). 2016 December ; 48: 43–50. doi:10.1016/j.dnarep.2016.10.010.

Enhanced Sensitivity of *Neil1*$^{-/-}$ Mice to Chronic UVB Exposure

Marcus J Calkins[1,*], **Vladimir Vartanian**[1], **Nichole Owen**[1], **Guldal Kirkali**[2,**], **Pawel Jaruga**[2], **Miral Dizdaroglu**[2], **Amanda K. McCullough**[1,3], and **Stephen R. Lloyd**[1,4,5]

[1]Oregon Institute of Occupational Health Sciences, Oregon Health & Science University Portland, Oregon 97239-3098

[2]Biomolecular Measurement Division, National Institute of Standards and Technology, Gaithersburg MD 20899-8311

[3]Department of Molecular and Medical Genetics, Oregon Health & Science University Portland, Oregon 97239-3098

[4]Department of Physiology and Pharmacology, Oregon Health & Science University Portland, Oregon 97239-3098

Abstract

Oxidative stress and reactive oxygen species (ROS)-induced DNA base damage are thought to be central mediators of UV-induced carcinogenesis and skin aging. However, increased steady-state levels of ROS-induced DNA base damage have not been reported after chronic UV exposure. Accumulation of ROS-induced DNA base damage is governed by rates of lesion formation and repair. Repair is generally performed by Base Excision Repair (BER), which is initiated by DNA glycosylases, such as 8-oxoguanine glycosylase and Nei-Endonuclease VIII-Like 1 (NEIL1). In the current study, UV light (UVB) was used to elicit protracted low-level ROS challenge in wild-type (WT) and *Neil1*$^{-/-}$ mouse skin. Relative to WT controls, *Neil1*$^{-/-}$ mice showed an increased sensitivity to tissue destruction from the chronic UVB exposure. Relative to WT skin, *Neil1*$^{-/-}$ mice experienced chronic inflammatory responses as measured by cytokine message levels and profiling, as well as neutrophil infiltration. Additionally, levels of several ROS-induced DNA lesions were measured including 4,6-diamino-5-formamidopyrimidine (FapyGua), 2,6-diamino-4-hydroxy-5-formamidopyrimidine (FapyAde), 8-hydroxyguanine (8-OH-Gua), 5,6-dihydroxyuracil (5,6-diOH-Ura) and thymine glycol (ThyGly). In WT mice, chronic UVB exposure led to increased steady-state levels of FapyGua, FapyAde, and ThyGly with no significant increases in 8-OH-Gua or 5,6-diOH-Ura. Interestingly, the lesions that accumulated were all substrates of NEIL1. Collectively, these data suggest that NEIL1-initiated repair of a subset of ROS-induced DNA base lesions may be insufficient during chronic UV exposure in mouse skin.

[5]corresponding author; 3181 SW Sam Jackson Park Rd. Portland, OR 97239, 503-494-9957 (voice), 503-494-6831 (fax), lloydst@ohsu.edu.
*Current address: Institute of Clinical Medicine, National Cheng Kung University, Tainan, Taiwan
**Current address: National Institutes of Health, National Cancer Institute, Bethesda, MD 20841

Conflict of Interest
The authors declare no conflict of interest.

Keywords

DNA base excision repair; DNA glycosylases; UV-induced inflammation; Oxidative DNA base damage

1. Introduction

Ultraviolet (UV) light exposures elicit complex biological responses in skin that ultimately lead to outcomes such as sunburn, immunosuppression, skin aging, and cancer. Many of the deleterious effects of UV light are attributable to DNA damage, and much attention has focused on DNA base damage that is directly produced by UV photon absorption. In particular, cyclobutane pyrimidine dimers (CPDs) are thought to mediate immune suppression [1, 2] as well as melanoma and non-melanoma skin cancer (reviewed in [3]). Although a role for oxidative DNA lesions in these processes has been suggested, the identity of these lesions has not been determined.

Light wavelengths ranging from 280 – 315 nm (UVB) are known to induce direct modifications on DNA, while wavelengths from 315 – 400 nm (UVA) are hypothesized to act through photosensitizers, leading to increased oxidative stress. However, recent evidence has blurred this distinction. For example, CPDs were found to be the predominant lesion in UVA exposed human skin cells and tissue [4, 5], which may be attributed to the presence of natural photosensitizers that generate long-lived radical species. In fact, it has been recently demonstrated that CPDs can be formed in DNA up to several hours following UVA irradiation via oxidation of melanin [6]. Other studies have shown that significant levels of 8-hydroxyguanine (8-OH-Gua) accumulate in DNA transiently after UVB exposure [7–11]. Further, UVB can directly induce several types of reactive oxygen species (ROS)-mediated DNA lesions, including 4,6-diamino-5-formamidopyrimidine (FapyAde), which is formed in DNA by irradiation at 310 nm in a dose dependent manner from 0.5 kJ/m^2 to 10 kJ/m^2 [12, 13]. Although 8-OH-Gua is the most commonly measured of these damages, a menagerie of lesions including FapyAde, 2,6-diamino-4-hydroxy-5-formamidopyrimidine (FapyGua), 5,6-dihydroxyuracil (5,6-diOH-Ura) and thymine glycol (ThyGly) are formed at comparable frequencies [14].

Oxidative stress is a well-established consequence of UVB exposure. In general, measurements of ROS-induced damage products reveal a time delay in the generation of the oxidative environment. For example, increases in F2-isoprostanes within the dermal interstitial space were shown 24 h following UVB exposure to human skin, but not immediately after exposure [15–17]. One plausible explanation for this time delay is that the immunological responses following UVB exposure are the primary mediators of ROS generation in the skin [18, 19]. Interestingly, while other measures of persistent oxidative stress are present in skin following UVB exposure, increased levels of oxidative DNA base damage have not been consistently reported. This lack of accumulation could potentially be attributed to efficient repair and removal of these lesions from the genome. However, UV-induced oxidative stress is known to contribute to carcinogenic processes, including mutagenesis (reviewed in [20]). Furthermore, mice deficient in 8-oxoguanine DNA

glycosylase (OGG1), which is primarily responsible for 8-OH-Gua repair, were more susceptible to UVB-induced skin carcinogenesis relative to OGG1-proficient mice [10, 21, 22]. Therefore, a role for ROS-induced DNA base lesions in skin carcinogenesis is implied, and persistent increases in such lesions may be expected.

In the current study, we assessed the levels of persistent ROS-induced DNA lesions in chronic UVB exposed mouse skin that may represent a state of chronic skin inflammation. For the first time, we show persistent accumulation of mutagenic and cytotoxic DNA lesions in mouse skin that was chronically exposed to UVB, and describe a potential role for NEIL1, in protecting from these accumulated lesions.

2. Materials and Methods

2.1 Animals

Neil1$^{-/-}$ mice were backcrossed on a C57Bl/6 background for 13 generations. WT and *Neil1*$^{-/-}$ female mice between 12 and 15 weeks of age were randomly divided and group housed up to five per cage. Animals were maintained under the regulations set forth by Oregon Health & Science University, Department of Comparative Medicine.

2.2 Ultraviolet light exposure

Mice were exposed to chronic UVB with a ramping dose using a Blak-Ray XX-15M UV bench lamp fitted with two F15T8 UV-B bulbs (UVP, Upland, CA). The UVB light source was set at a distance such that the dorsal surface of each mouse received 1.1 mW/cm^2. Mice were exposed three times per week, according to a ramping protocol, such that during the first week, mice received 0.5 kJ/m^2 at each dose, while in subsequent weeks, the dose was increased to 1, 1.5, 2, 3, 4, 5, 6, 7, 8, 9, and finally 10 kJ/m^2. Once mice reached 10 kJ/m^2, the dose was maintained for 10 weeks. Animals were sacrificed 3 days following the last dose and whole skin samples, including epidermis, dermis, and subcutaneous fat were collected. Tissue samples (approximately 1 cm^2) were taken from similar dorso-caudal locations for histological examination. The remaining portions of the dorsal skin were scraped to remove sub-dermal tissue and collected into liquid nitrogen for biochemical analyses. Quantitative measurements of skin thickness were made using Image J software. Hematoxylin and eosin (H&E) staining was performed by the Histopathology Shared Resources Core at OHSU.

2.3 Quantitative RT-PCR

Frozen skin samples were pulverized under liquid nitrogen using a ceramic mortar and pestle. A random subset of 8 animals from each UVB exposed group was selected for analyses. From each mouse, ~50 mg of pulverized tissue was weighed and suspended in 1 mL of TRIzol reagent. Samples were homogenized with an OMNI tissue grinder with serrated stainless steel tip at 200 rpm for three bursts of 20 s and frozen at −80 °C. After thawing, homogenized samples were spun at 12,000 g for 10 min to separate TRIzol from both extracellular matrix (pellet) and excess fat (floating on supernatant). Total RNA was isolated by the standard TRIzol method according to manufacturer's instructions. One μg of total RNA was used to synthesize cDNA. First-strand cDNA synthesis was made using

SuperScript II RT reactions (Invitrogen). Oligo-dT primers (500 ng), total RNA (1 μg), and dNTP (10 pmol each) in 12 μL were heated to 65 °C for 5 min and then placed on ice, after which 4 μl of 5X First-Strand buffer, 2 μL of 0.1 M DTT, and 1 μL of RNaseOUT were added. The mixture was incubated at 42 °C for 2 min, and 1 μL of SuperScript II RT was added. The reaction was incubated at 42 °C for 50 min and then inactivated by heating to 70 °C for 15 min. Samples were diluted with 180 μL of nuclease-free water.

Gene expression levels were determined by qPCR using SYBR Green Supermix (BioRad). Primers were used at a 240 nM final concentration and annealing temperature was 55 °C for all primer pairs. C_t data were collected from 4 μL of cDNA on a BioRad iCycler. Data were analyzed using the $\Delta\Delta C_t$ method with untreated wild-type skin serving as the control. Primers were developed for CXCL5, gp91phox, gp67phox, Mac1, IL-22, IL-10, IL-6, IL-4, IL-1β, IL-1α, IFNγ, TNFα, NEIL1, NEIL2, OGG1, NTH1, and ribosomal subunit ABRP was used for normalization.

2.4 Plasma cytokine determination

Blood was harvested from mice at the time of sacrifice by cardiac puncture into EDTA containing tubes. Plasma was separated by centrifugation at 4000 g for 4 min. Circulating cytokine levels were determined from plasma using a Mouse Cytokine Magnetic 10-plex Panel (Invitrogen) on a Luminex 200 cytometer (Luminex Corp, Austin, TX) according to manufacturer's instructions. Flow cytometry was performed by the OHSU Flow Cytometry Shared Resource.

2.5 Immunohistochemistry

Skin sections were formalin-fixed and paraffin-embedded, with immunohistochemistry performed at the OHSU Histopathology Core as follows. Slides were stained using the Ventana Benchmark XT automated IHC stainer. Briefly, slides were baked for 1 hr at 60 °C, then loaded onto the Ventana, where all subsequent steps were performed. Antigen retrieval was done at 98 °C for 30 min, and slides incubated in primary antibody to Ly-6G/Ly-C6 for 32 min at 37 °C (BD Pharmingen). Following a peroxidase block, slides were incubated in goat-α-rat-horseradish peroxidase (ImmPRESS) and 3,3′-diaminobenzidine (DAB) (Ventana). Slides were counterstained with hematoxylin, dehydrated through alcohol washes, and cleared with xylene. Tissues were imaged on a Zeiss ApoTome2 upright Microscope with a Zeiss AxioCam 506 CCD color camera. Images were taken with the 20x objective and a uniform exposure using Zen (Zeiss) software. Ten images per animal were taken from random fields, and from at least two sections of skin. All images were analyzed using FIJI (Image J) software and subjected to color deconvolution and identical linear brightness correction. Background DAB levels were accounted for using multiple fields of the IgG control. Thresholding was applied to determine DAB positive cells in each field and manually counted. Apparent cross-reactivity of the antibody with hair follicles was not taken into consideration when counting positive cells, though these cells are apparent on representative images. They are distinguishable from neutrophils based on location (in bulb) and morphology.

2.6 DNA isolation

Frozen skin samples were pulverized under liquid nitrogen with a ceramic mortar and pestle. A random subset of 5 animals from each UVB-exposed group was selected for analyses. Approximately 200 mg of tissue was weighed into a 1.5 mL microcentrifuge tube and suspended in 1 mL of tissue lysis buffer (10 mM Tris pH 8.2, 2 mM EDTA, 400 mM NaCl, 1% SDS) with Proteinase K (2 mg/ml final concentration) and incubated at 37 °C overnight. A total of 250 μL of 5 M NaCl was added and then samples were centrifuged at 12,000 g for 15 min at 4 °C. The supernatant was transferred to a 15 mL conical tube and 2.5 mL of 100% ethanol added. DNA was allowed to precipitate overnight at −20 °C. The pellet was resuspended into 1 mL TE buffer with Proteinase K (2 mg/mL) and incubated at 55 °C for 1 h. 250 μL of 5 M NaCl was added and then samples were centrifuged at 12,000 g for 15 min at 4 °C. The supernatant was transferred to a 15 mL conical tube and DNA was precipitated at −20 °C overnight after addition of 2.5 mL 100% ethanol. The DNA pellet was dried and stored in 70% ethanol.

2.7 Measurements of DNA base lesions

ROS-induced DNA base lesions were measured by gas chromatograph-tandem mass spectrometry (GC-MS/MS) with isotope dilution. The methodology has been previously described in detail [14, 23].

2.8 Statistics

Data were analyzed by two-way ANOVA with post-hoc Bonferroni comparison. Values of $p < 0.05$ were considered statistically significant. Graphical data are presented as mean ± standard deviation, except where noted in the figure legend.

3. Results

3.1 WT and Neil1$^{-/-}$ mice skin response to chronic UVB exposure

Preliminary studies in shaved WT and *Neil1*$^{-/-}$ mice using 10 kJ/m^2 UVB produced excessive skin abrasions primarily in *Neil1*$^{-/-}$ mice. Thus, exposure protocols were revised such that mice were exposed to UVB *via* a ramping dose with three exposures per week. Over the course of 12 weeks, the exposure was increased from 0.5 kJ/m^2 to 10 kJ/m^2 per exposure. Once the dose reached 10 kJ/m^2, it was maintained for 10 weeks for a total exposure time of 22 weeks. WT mice easily tolerated the schedule, developing thickened skin with periodic mild abrasions on the exposed tissue. These small abrasions were transient and typically resolved within one week. In contrast, the *Neil1*$^{-/-}$ mice developed more severe abrasions that would periodically resolve and return throughout the protocol, again suggesting that *Neil1*$^{-/-}$ mice exhibit an increased sensitivity to UVB. Even with this very gradual dose escalation, during the course of the study, three of the original 20 *Neil1*$^{-/-}$ mice required euthanasia with abraded skin that was recalcitrant to healing over 50% of their dorsal surface. The *Neil1*$^{-/-}$ mice showed increased propensity toward excoriation and abrasion and a qualitative increase in skin rigidity in the non-abraded areas. Overall, a clear difference was observed in the nature of skin damage between the WT and *Neil1*$^{-/-}$ mice.

Morphological changes in epidermal and dermal thicknesses were qualitatively evaluated from H&E stained sections (Fig. 1a). As shown at a higher magnification, increased numbers of keratinocytes and dermal fibrosis were clearly visible in samples from virtually all UVB exposed animals (Fig. 1b). Quantitative measurements confirmed that epidermal thickness of UVB exposed skin was increased as compared to unexposed control animals in both WT and *Neil1*$^{-/-}$ mice (Fig. 1c). Interestingly, epidermal thickness in the non-abraded tissue from UVB exposed *Neil1*-deficient animals was greater than UVB exposed WT mice. Stratum corneum thickness and density also appeared to be increased after UVB exposure, but these data were not quantified. Additionally, although dermal thickness was not different between unexposed and exposed WT mice, dermal thickness was increased in *Neil1*$^{-/-}$ mice after UVB exposure (Fig. 1d).

3.2 UVB exposure causes chronic, low-level inflammation

Since the *Neil1*$^{-/-}$ mice showed enhanced morphological alterations consistent with chronic UVB-induced inflammation, expression levels of several inflammation-related genes were examined (Fig. 2a). Homogenized skin samples were analyzed by quantitative PCR for markers of the following: i) infiltrating leukocytes (gp91phox, gp67phox, CD11b/Mac1), ii) anti-inflammatory processes (IL-4, IL-10), iii) pro-inflammatory processes (TNFα, IFNγ, IL-1α, IL-1β, IL-6), iv) keratinocyte proliferation signaling (IL-22), and v) generalized UV response (CXCL5; which mitigates sunburn pain). UVB-irradiated WT mice showed minimal increases in most of these markers with IL-4, IL-1β, and CXCL5 the only three that displayed statistically significant increases (Fig. 2a). In contrast, significant increases were detected in nine of the twelve genes in skin of *Neil1*$^{-/-}$ mice that were exposed to UVB. The gene with the greatest differential expression levels between WT and *Neil1*$^{-/-}$ skin was IL-22 (0.9 and 13.9-fold, respectively).

In order to measure systemic inflammation, plasma samples were harvested from mice prior to sacrifice and analyzed for multiple cytokines with a mouse cytokine magnetic 10-plex panel. The panel included anti-inflammatory cytokines (IL-2, IL-4, and IL-10) as well as pro-inflammatory cytokines (GM-CSF, IFN-γ, IL-1β, IL-5, IL-6, IL-12, and TNFα). Of these cytokines, IL-6 and TNFα were found to be elevated in both WT and *Neil1*$^{-/-}$ mice after UVB exposure while IL-4 and GM-CSF were upregulated in *Neil1*$^{-/-}$ and WT mice respectively (Fig. 2b). Overall, the results indicate that WT and *Neil1*$^{-/-}$ mice experience chronic inflammatory processes both systemically and in the exposed skin. In skin, inflammatory processes were more easily observed in *Neil1*$^{-/-}$ mice compared to WT. The overall increased inflammatory response in *Neil1*$^{-/-}$ mice may reflect the observed increased rate of tissue destruction after chronic UVB exposure.

The relative state of inflammation within the skin was further characterized by immunostaining for neutrophil invasion using the Ly6C/Ly6G marker for monocytes, granulocytes and neutrophils (Fig 3a and 3b). These cells have been previously implicated as the major source of oxidative stress in chronic UVB exposed skin tissue [18, 19]. In UVB exposed WT mice and *Neil1*$^{-/-}$ mice, statistically significant increases in the number of neutrophils were found compared to unexposed animals of the same genotype. Furthermore, UVB-exposed *Neil1*$^{-/-}$ mouse skin had increased neutrophil content compared to UVB-

exposed WT skin, but there were no differences between genotype in the unexposed animals (Fig 3a). Of note, the invading immune cells were typically associated with the basal layer of the epidermis (Fig 3b). These data correspond to the histological features of the skin and inflammatory cytokines in the skin and plasma. Thus, the observed neutrophil invasion indicates the presence of a chronic source for ROS in UVB-exposed mouse skin that was exaggerated by the *Neil1* deficiency.

3.3 Accumulation of ROS-induced DNA base damage in skin

Given the morphological and cytokine evidence for differential UVB responsiveness between WT and *Neil1*$^{-/-}$ mice, ROS-induced DNA lesions were measured by GC-MS/MS with isotope dilution in DNA isolated from un-irradiated and irradiated skin from both genotypes. Statistically significant differences in the levels of spontaneous base damage (in unexposed skin tissue) were observed for FapyAde, ThyGly, and FapyGua (Fig. 4a, 4b, 4c, respectively) between WT and *Neil1*$^{-/-}$ mice. No differences in the levels of 5,6-diOH-Ura or 8-OH-Gua were found between WT and *Neil1*$^{-/-}$ (Fig. 4d, 4e, respectively).

Chronic UVB exposure resulted in significantly increased levels of FapyAde, ThyGly, and FapyGua in WT mice (Fig. 4a, 4b, and 4c, respectively). This result was unanticipated since BER repair of ROS-induced lesions is extremely efficient. Therefore, the observed increase in damage may be attributable to a persistent oxidative environment in chronically exposed skin, coupled with an insufficient BER response. Levels of 5,6-diOH-Ura and 8-OH-Gua were unaffected by UVB exposure, possibly indicating sufficiency of BER directed toward these lesions. *Neil1*$^{-/-}$ mouse skin did not significantly accumulate additional ROS-induced DNA lesions as a result of the chronic UVB exposure regimen, although some increases in the levels of FapyAde and FapyGua were observed, possibly indicating a threshold for DNA damage within the skin. It may be speculated that levels of DNA lesions above the threshold may induce the tissue destruction that was described above.

Since rates of spontaneous depurination or depyrimidination are negligible for the analyzed lesions, the steady-state levels are predominantly determined by their formation and elimination by repair. FapyGua, FapyAde, and ThyGly are all known to be repaired by NEIL1, NEIL2, NEIL3 and NTH1 (NEI/NTH glycosylases), whereas 8-OH-Gua is repaired by OGG1 only. Therefore, the data may indicate that in WT mice, 8-OH-Gua repair by OGG1 is sufficient to maintain low levels of the lesion. However, rates of repair for FapyAde, FapyGua and ThyGly in the skin of WT mice may be insufficient to eliminate all of these lesions.

4. Discussion

Solar UV exposure stimulates a biphasic oxidative response in skin. The first phase consists of ROS that are generated in UVA exposed cells by photosensitizing molecules. The second phase arises from UVA/B-induced infiltration of immune cells [15, 24–27]. During chronic UV exposure, skin tissue adapts to decrease the effective UV dose by hyper-proliferation of keratinocytes and thickening of the stratum corneum, as well as increased melanin production. In addition, UV light induces an immune tolerance response that is at least partially produced via recruitment of T-regulatory cells to skin tissue [28, 29]. However,

prolonged low-level inflammatory processes still occur. The major source for ROS after UVB exposure is thought to be infiltrating CD11b+ leukocytes in both human and mouse skin [18, 19]. Both macrophages and neutrophil granulocytes that express NADPH oxidase are marked by CD11b, and are likely sources of ROS during the respiratory burst phase of activation. In the current experiments, chronic UVB exposure produced expected changes in tissue composition, including evidence for chronic inflammation that would be suggestive of a persistent oxidative environment.

In UVB-exposed skin, the only cytokine that showed major expression differences between WT and *Neil1*$^{-/-}$ was IL-22 (0.9 and 13.9-fold, respectively). Given its role in stimulating the JAK/STAT response pathway in keratinocytes and thereby eliciting cellular proliferation [30], the elevated level in *Neil1*$^{-/-}$ mice is consistent with the previously noted persistent epidermal hyperplasia. Interestingly, statistically significant increases in induction of both pro- and anti-inflammatory cytokines were observed in UVB-exposed mouse skin. The largest upregulations were observed for the highly pleiotropic [31] pro-inflammatory cytokine IL-1β. On the other hand, increases in IL-4 expression were observed in both WT and *Neil1*$^{-/-}$ animals after UVB exposure (2.4 and 4.8-fold respectively). Since IL-4 promotes macrophage transition to an M2 phenotype [32], this result suggests that at the time of sacrifice, in both genotypes the immune reaction may have been transitioning toward healing response rather than inflammation. In mouse plasma, IL-6 and TNFα were up-regulated in both WT and *Neil1*$^{-/-}$ animals after exposure. GM-CSF and IL-4 were elevated in both genotypes after UVB exposure, however this elevation only reached statistical significance in WT and *Neil1*$^{-/-}$ respectively. GM-CSF is known to induce proliferation of monocytes, which can then migrate into tissues and differentiate into macrophages. Coupled to this response, increased levels of IL-4 are expected to drive the previously mentioned M2 response. Systemic elevation of both pro- and anti-inflammatory cytokines corroborates the RT-PCR data from skin tissue and may reflect an overall transition toward healing response. As such, the elevations in IL-6 and TNFα may represent residual pro-inflammatory responses that arose from the repeated UV-induced tissue damage.

This mixed pro- and anti-inflammatory environment likely led to increased oxidative stress in the skin tissue and formation of ROS-induced DNA base lesions. In accordance with this hypothesis, we see evidence of neutrophil invasion in UVB-exposed WT and *Neil1*$^{-/-}$ tissues, indicating that NADPH oxidase activity might contribute to chronic ROS exposure. With the exception of 8-OH-Gua, measurements of ROS-induced DNA base lesions have not been previously reported after chronic doses of UVB. In those studies that did examine 8-OH-Gua, a transient elevation of base damage was observed without severe tissue injury. In one study, elevated levels of 8-OH-Gua were found in HOS:Hr-1 albino mouse skin that was chronically treated with 2 or 10 MED UVB three times per week and harvested immediately after the final UVB exposure [7]. This elevation of 8-OH-Gua corresponded with increased levels of 3-nitro-L-tyrosine, a hallmark of inflammatory response that suggested the inflammatory processes can mediate 8-OH-Gua formation. In an apparent contrast, our data show that 8-OH-Gua was not persistently elevated 72 hr following the final UVB exposure. Of note, 8-OH-Gua levels in the previous study were measured using HPLC with electrochemical detection of 8-OH-dG (2′-deoxynucleoside form of 8-OH-Gua) and also immunohistochemical detection [7]. Compared to the GC-MS/MS isotope-dilution method

employed in the current study, these methods are not as specific or accurate for quantification of DNA lesions. Furthermore, no internal standards are used to positively identify the lesion of interest with either the HPLC or immunostaining method. Despite these methodological concerns, the apparently incongruous results may be explained if OGG1 mediated repair of 8-OH-Gua is more efficient than NEI/NTH mediated repair of FapyAde, FapyGua, and ThyGly. In this situation, a higher load of chronic ROS would be required in the tissue to observe increased steady state levels of 8-OH-Gua levels compared to the other lesions. Thus, the differences in mouse strain and exposure protocols could easily explain the contrasting results.

In another study, 24 hr after a single dose of 3 kJ/m^2 UVB, no increased level of 8-OH-Gua was found in C57BL/6J, WT mice [10]. In the same manuscript, the authors also examined 8-OH-Gua after chronic UVB exposure. In this study, the lesion clearly increased only in *Ogg1*$^{-/-}$ mice and not in WT mice chronically exposed to UVB, suggesting the efficient repair of 8-OH-Gua [10]. However, although another report showed persistent elevation of 8-OH-Gua levels after UVB exposure, this study utilized an extremely high dose [8], which likely caused severe inflammation and tissue damage. 8-OH-Gua levels are known to rapidly increase and then return to baseline within 2 hr in HaCaT cells following either 30 kJ/m^2 UVA or 1.5 kJ/m^2 UVB exposure [9]. Although this time course may be slightly prolonged in epidermal tissue [11], previous literature suggests that 8-OH-Gua lesions are efficiently repaired by OGG1 and subsequent BER steps in chronic UVB-exposed skin.

In stark contrast, our data clearly show persistent accumulation of FapyAde, FapyGua and ThyGly after chronic UVB exposure. These findings are on a par with the fact that 8-OH-Gua is repaired by OGG1 only, whereas FapyAde, FapyGua and ThyGly are the substrates of NEIL1, which does not act on 8-OH-Gua. Furthermore, our data suggest that these lesions may be more relevant than 8-OH-Gua for generating the detrimental processes which result from UV exposure. Importantly, measurements made in simian kidney cells showed that FapyGua is more mutagenic than 8-OH-Gua [33], and ThyGly is a well-known strong block to replicative polymerases [34–37] or mutation causing lesion if translesion synthesis is performed by polymerase θ [38]. Thus, persistent accumulation of lesions such as these may explain the previously described carcinogenic accumulation of ROS-derived mutations in UV exposed skin [20]. It is also possible that accumulated DNA base lesions could participate in skin aging, through a mechanism that is still undetermined. Previous experiments have shown that *Neil1*$^{-/-}$ mice harbor a baseline accumulation of FapyAde and FapyGua in tissues including brain, kidney, and liver [39, 40]. Our data confirm this baseline accumulation in skin tissue and suggest that *Neil1*$^{-/-}$ mice may be more susceptible to disease states, such as carcinogenesis, in which DNA damage is critical, as was previously observed in *Neil1*$^{-/-}$ mice [39, 40]. We observed some, but not statistically significant accumulation of FapyAde and FapyGua in *Neil1*$^{-/-}$ mice following UVB irradiation in contrast to WT mice. The levels of FapyAde and FapyGua in *Neil1*$^{-/-}$ mice were already almost as high as those in irradiated WT mice. The low dose UVB irradiation may not have caused any detectable additional increase in the levels of these lesions in *Neil1*$^{-/-}$ mice. This lack of increase may also be due to tissue destruction and healing response observed in the *Neil1*$^{-/-}$ mice. Interestingly, *Neil1*$^{-/-}$ mouse skin did not accumulate additional ROS-induced DNA lesions as a result of the chronic UVB exposure regimen. However, this

comparative analysis of UVB-induced DNA base damage in the skin of *Neil1*$^{-/-}$ mice should be tempered due to the high frequency of excoriation and skin loss after UVB exposure. Owing to the major differences in skin composition between irradiated *Neil1*$^{-/-}$ and the other experimental groups, possible interpretations of these data are limited.

It is likely that increased tissue destruction in *Neil1*$^{-/-}$ mouse skin limits the accumulation of ROS-induced DNA lesions after chronic UVB exposure. Without the photosensitivity, we expect that Nei1-substrate lesions would have drastically increased in the chronic UVB exposed tissues. The reason for this tissue destruction was not determined, but may be speculated. One possibility is that in the inflammatory/oxidative environment created by chronic UVB, *Neil1*$^{-/-}$ cells more easily exceed the threshold of DNA lesions necessary to initiate apoptosis, and thus contribute to the observed sensitivity. Another possible explanation is related to the previously reported metabolic syndrome which develops in aged *Neil1*$^{-/-}$ mice [41, 42]. Clear associations between metabolic diseases and UV exposures have been made by others. For example, in Smith-Lemli-Opitz patients with cholesterol biosynthesis defects, photosensitivity to UVA has been reported [43, 44]. Additionally, defective heme biosynthesis, primarily in liver, may lead to the systemic accumulation of porphyrins and thereby contribute to photosensitivity [45, 46]. Moreover, broadband UV exposure was found to relieve metabolic syndrome in C57Bl/6 mice that were fed with a high fat diet. Interestingly, this phenomenon was not dependent on vitamin D, but instead was related to nitric oxide production [47]. Thus, it is possible that the metabolic syndrome that develops in *Neil1*$^{-/-}$ mice either confers or is mechanistically linked to the observed photosensitivity. Further studies will be required to evaluate these potential links and elucidate the mechanism of *Neil1*$^{-/-}$ sensitivity to UVB and any potential links to metabolic disease.

The influence of OGG1 in prevention of UVB-mediated carcinogenesis has been investigated. In a pair of studies published by Kunisada et al. [10, 21], the effect of deficient repair of ROS-induced DNA damage was studied in UVB-induced carcinogenesis. *Ogg1*$^{-/-}$ mice developed tumors earlier and in increased numbers relative to WT and heterozygous mice [10]. Surprisingly, *Ogg1*$^{-/-}$ mice that were irradiated with narrow band UVB were not different compared to WT in latency of tumor formation, tumor burden, or percentage of malignant tumors. These results suggested that broad-band UVB, as opposed to narrow band-UVB, induced oxidative damage and that this oxidative damage was important in carcinogenesis [21]. Moreover, the carcinogenesis phenotype in *Ogg1*$^{-/-}$ mice was not shown to result from increased mutagenesis within the keratinocytes, but rather a stimulation of immune response *via* secretion of an extracellular matrix protein, versican. Versican content was highly correlated with increased neutrophil residence in both human tumors and mouse models [22]. Our study could not address carcinogenicity in *Neil1*$^{-/-}$ mice due to the severity of overall tissue destruction in exposed skin. Future studies, utilizing *Neil1*$^{-/-}$ hairless mice, exposed to solar-simulated UV light will be most appropriate to further understand role of NEIL1 in UV-induced skin carcinogenesis. However, our data do suggest that *Neil1*$^{-/-}$ mice exhibit an enhanced immune response and overall tissue sensitivity after chronic UVB exposure, which may contribute to carcinogenic processes. In addition, our finding that WT mice accumulate FapyAde, FapyGua and ThyGly lesions after chronic

UVB exposure implies that repair of these specific lesions may be critical in determining the fate of UV exposed skin.

5. Conclusions

For the first time, increased steady-state levels of ROS-induced DNA lesions have been measured following chronic UVB exposure. In contrast to 8-OH-Gua, three oxidative lesions including FapyAde, FapyGua and ThyGly were elevated in mouse skin that was chronically exposed to UVB. This steady-state elevation implies that these lesions may be largely responsible for the ROS-induced mutations seen in UV carcinogenesis. Moreover, because of the mutagenic and cytotoxic potentials, these specific lesions may be highly relevant to immunosuppression and UV light-induced aging as well. Since we have observed a selective and persistent accumulation of DNA lesions normally repaired by NEI/NTH glycosylases after chronic UVB exposure, augmentation of these repair pathways may represent a viable prevention strategy for skin carcinogenesis.

Acknowledgments

The Training Program in the Molecular Basis of Skin/Mucosa Pathobiology (T32-CA106195) supported MJC.

Abbreviations

UV	ultraviolet
ROS	reactive oxygen species
CPD	cyclobutane pyrimidine dimer
8-OH-Gua	8-hydroxyguanine
FapyGua	2,6-diamino-4-hydroxy-5-formamidopyrimidine
FapyAde	4,6-diamino-5-formamidopyrimidine
5,6-diOH-Ura	5,6-dihydroxyuracil
ThyGly	thymine glycol
BER	base excision repair
H&E	hematoxylin and eosin
WT	wild type
IL	interleukin
IFN	interferon
TNF	tumor necrosis factor
CXCL	Chemokine (C-X-C Motif) Ligand

References

1. Kripke ML, Cox PA, Alas LG, Yarosh DB. Pyrimidine dimers in DNA initiate systemic immunosuppression in UV-irradiated mice. Proc Natl Acad Sci U S A. 1992; 89:7516–7520. [PubMed: 1502162]
2. Wolf P, Yarosh DB, Kripke ML. Effects of sunscreens and a DNA excision repair enzyme on ultraviolet radiation-induced inflammation, immune suppression, and cyclobutane pyrimidine dimer formation in mice. J Invest Dermatol. 1993; 101:523–527. [PubMed: 8409517]
3. Pfeifer GP, Besaratinia A. UV wavelength-dependent DNA damage and human non-melanoma and melanoma skin cancer. Photochem Photobiol Sci. 2012; 11:90–97. [PubMed: 21804977]
4. Mouret S, Baudouin C, Charveron M, Favier A, Cadet J, Douki T. Cyclobutane pyrimidine dimers are predominant DNA lesions in whole human skin exposed to UVA radiation. Proc Natl Acad Sci U S A. 2006; 103:13765–13770. [PubMed: 16954188]
5. Courdavault S, Baudouin C, Charveron M, Favier A, Cadet J, Douki T. Larger yield of cyclobutane dimers than 8-oxo-7, 8-dihydroguanine in the DNA of UVA-irradiated human skin cells. Mutat Res. 2004; 556:135–142. [PubMed: 15491641]
6. Premi S, Wallisch S, Mano CM, Weiner AB, Bacchiocchi A, Wakamatsu K, Bechara EJ, Halaban R, Douki T, Brash DE. Photochemistry. Chemiexcitation of melanin derivatives induces DNA photoproducts long after UV exposure. Science. 2015; 347:842–847. [PubMed: 25700512]
7. Hattori Y, Nishigori C, Tanaka T, Uchida K, Nikaido O, Osawa T, Hiai H, Imamura S, Toyokuni S. 8-hydroxy-2′-deoxyguanosine is increased in epidermal cells of hairless mice after chronic ultraviolet B exposure. J Invest Dermatol. 1996; 107:733–737. [PubMed: 8875958]
8. Hattori-Nakakuki Y, Nishigori C, Okamoto K, Imamura S, Hiai H, Toyokuni S. Formation of 8-hydroxy-2′-deoxyguanosine in epidermis of hairless mice exposed to near-UV. Biochem Biophys Res Commun. 1994; 201:1132–1139. [PubMed: 8024554]
9. Javeri A, Lyons JG, Huang XX, Halliday GM. Downregulation of Cockayne syndrome B protein reduces human 8-oxoguanine DNA glycosylase-1 expression and repair of UV radiation-induced 8-oxo-7, 8-dihydro-2′-deoxyguanine. Cancer Sci. 2011; 102:1651–1658. [PubMed: 21668583]
10. Kunisada M, Sakumi K, Tominaga Y, Budiyanto A, Ueda M, Ichihashi M, Nakabeppu Y, Nishigori C. 8-Oxoguanine formation induced by chronic UVB exposure makes Ogg1 knockout mice susceptible to skin carcinogenesis. Cancer Res. 2005; 65:6006–6010. [PubMed: 16024598]
11. Wei H, Cai Q, Tian L, Lebwohl M. Tamoxifen reduces endogenous and UV light-induced oxidative damage to DNA, lipid and protein in vitro and in vivo. Carcinogenesis. 1998; 19:1013–1018. [PubMed: 9667739]
12. Kielbassa C, Roza L, Epe B. Wavelength dependence of oxidative DNA damage induced by UV and visible light. Carcinogenesis. 1997; 18:811–816. [PubMed: 9111219]
13. Doetsch PW, Zasatawny TH, Martin AM, Dizdaroglu M. Monomeric base damage products from adenine, guanine, and thymine induced by exposure of DNA to ultraviolet radiation. Biochemistry. 1995; 34:737–742. [PubMed: 7827031]
14. Dizdaroglu M, Kirkali G, Jaruga P. Formamidopyrimidines in DNA: mechanisms of formation, repair, and biological effects. Free Radic Biol Med. 2008; 45:1610–1621. [PubMed: 18692130]
15. Grundmann JU, Wiswedel I, Hirsch D, Gollnick HP. Detection of monohydroxyeicosatetraenoic acids and F2-isoprostanes in microdialysis samples of human UV-irradiated skin by gas chromatography-mass spectrometry. Skin Pharmacol Physiol. 2004; 17:37–41. [PubMed: 14755126]
16. Wiswedel I, Grundmann JU, Boschmann M, Krautheim A, Bockelmann R, Peter DS, Holzapfel I, Gotz S, Muller-Goymann C, Bonnekoh B, Gollnick HP. Effects of UVB irradiation and diclofenac on F2-isoprostane/prostaglandin concentrations in keratinocytes and microdialysates of human skin. J Invest Dermatol. 2007; 127:1794–1797. [PubMed: 17330133]
17. Schneider LA, Bloch W, Kopp K, Hainzl A, Rettberg P, Wlaschek M, Horneck G, Scharffetter-Kochanek K. 8-Isoprostane is a dose-related biomarker for photo-oxidative ultraviolet (UV) B damage in vivo: a pilot study with personal UV dosimetry. Br J Dermatol. 2006; 154:1147–1154. [PubMed: 16704647]

18. Katiyar SK, Mukhtar H. Green tea polyphenol (−)-epigallocatechin-3-gallate treatment to mouse skin prevents UVB-induced infiltration of leukocytes, depletion of antigen-presenting cells, and oxidative stress. J Leukoc Biol. 2001; 69:719–726. [PubMed: 11358979]
19. Mittal A, Elmets CA, Katiyar SK. CD11b+ cells are the major source of oxidative stress in UV radiation-irradiated skin: possible role in photoaging and photocarcinogenesis. Photochem Photobiol. 2003; 77:259–264. [PubMed: 12685652]
20. Halliday GM. Inflammation, gene mutation and photoimmunosuppression in response to UVR-induced oxidative damage contributes to photocarcinogenesis. Mutat Res. 2005; 571:107–120. [PubMed: 15748642]
21. Kunisada M, Kumimoto H, Ishizaki K, Sakumi K, Nakabeppu Y, Nishigori C. Narrow-band UVB induces more carcinogenic skin tumors than broad-band UVB through the formation of cyclobutane pyrimidine dimer. J Invest Dermatol. 2007; 127:2865–2871. [PubMed: 17687389]
22. Kunisada M, Yogianti F, Sakumi K, Ono R, Nakabeppu Y, Nishigori C. Increased expression of versican in the inflammatory response to UVB- and reactive oxygen species-induced skin tumorigenesis. Am J Pathol. 2011; 179:3056–3065. [PubMed: 22001346]
23. Reddy PT, Jaruga P, Kirkali G, Tuna G, Nelson BC, Dizdaroglu M. Identification and quantification of human DNA repair protein NEIL1 by liquid chromatography/isotope-dilution tandem mass spectrometry. J Proteome Res. 2013; 12:1049–1061. [PubMed: 23268652]
24. Shindo Y, Witt E, Packer L. Antioxidant defense mechanisms in murine epidermis and dermis and their responses to ultraviolet light. J Invest Dermatol. 1993; 100:260–265. [PubMed: 8440901]
25. Shindo Y, Witt E, Han D, Packer L. Dose-response effects of acute ultraviolet irradiation on antioxidants and molecular markers of oxidation in murine epidermis and dermis. J Invest Dermatol. 1994; 102:470–475. [PubMed: 8151122]
26. Shindo Y, Witt E, Han D, Tzeng B, Aziz T, Nguyen L, Packer L. Recovery of antioxidants and reduction in lipid hydroperoxides in murine epidermis and dermis after acute ultraviolet radiation exposure. Photodermatol Photoimmunol Photomed. 1994; 10:183–191. [PubMed: 7880756]
27. Kuhn M, Wolber R, Kolbe L, Schnorr O, Sies H. Solar-simulated radiation induces secretion of IL-6 and production of isoprostanes in human skin in vivo. Arch Dermatol Res. 2006; 297:477–479. [PubMed: 16491351]
28. Schwarz T, Beissert S. Milestones in photoimmunology. J Invest Dermatol. 2013; 133:E7–E10.
29. Ullrich SE, Byrne SN. The immunologic revolution: photoimmunology. J Invest Dermatol. 2012; 132:896–905. [PubMed: 22170491]
30. Boniface K, Bernard FX, Garcia M, Gurney AL, Lecron JC, Morel F. IL-22 inhibits epidermal differentiation and induces proinflammatory gene expression and migration of human keratinocytes. J Immunol. 2005; 174:3695–3702. [PubMed: 15749908]
31. Feldmeyer L, Werner S, French LE, Beer HD. Interleukin-1, inflammasomes and the skin. Eur J Cell Biol. 2010; 89:638–644. [PubMed: 20605059]
32. Sica A, Mantovani A. Macrophage plasticity and polarization: in vivo veritas. J Clin Invest. 2012; 122:787–795. [PubMed: 22378047]
33. Kalam MA, Haraguchi K, Chandani S, Loechler EL, Moriya M, Greenberg MM, Basu AK. Genetic effects of oxidative DNA damages: comparative mutagenesis of the imidazole ring-opened formamidopyrimidines (Fapy lesions) and 8-oxo-purines in simian kidney cells. Nucleic Acids Res. 2006; 34:2305–2315. [PubMed: 16679449]
34. Clark JM, Beardsley GP. Functional effects of cis-thymine glycol lesions on DNA synthesis in vitro. Biochemistry. 1987; 26:5398–5403. [PubMed: 3676259]
35. McNulty JM, Jerkovic B, Bolton PH, Basu AK. Replication inhibition and miscoding properties of DNA templates containing a site-specific cis-thymine glycol or urea residue. Chem Res Toxicol. 1998; 11:666–673. [PubMed: 9625735]
36. Ide H, Kow YW, Wallace SS. Thymine glycols and urea residues in M13 DNA constitute replicative blocks in vitro. Nucleic Acids Res. 1985; 13:8035–8052. [PubMed: 3906566]
37. Aller P, Rould MA, Hogg M, Wallace SS, Doublie S. A structural rationale for stalling of a replicative DNA polymerase at the most common oxidative thymine lesion, thymine glycol. Proc Natl Acad Sci U S A. 2007; 104:814–818. [PubMed: 17210917]

38. Yoon JH, Roy Choudhury J, Park J, Prakash S, Prakash L. A role for DNA polymerase theta in promoting replication through oxidative DNA lesion, thymine glycol, in human cells. J Biol Chem. 2014; 289:13177–13185. [PubMed: 24648516]

39. Jaruga P, Xiao Y, Vartanian V, Lloyd RS, Dizdaroglu M. Evidence for the involvement of DNA repair enzyme NEIL1 in nucleotide excision repair of (5′R)- and (5′S)-8, 5′-cyclo-2′-deoxyadenosines. Biochemistry. 2010; 49:1053–1055. [PubMed: 20067321]

40. Chan MK, Ocampo-Hafalla MT, Vartanian V, Jaruga P, Kirkali G, Koenig KL, Brown S, Lloyd RS, Dizdaroglu M, Teebor GW. Targeted deletion of the genes encoding NTH1 and NEIL1 DNA N-glycosylases reveals the existence of novel carcinogenic oxidative damage to DNA. DNA Repair (Amst). 2009; 8:786–794. [PubMed: 19346169]

41. Vartanian V, Lowell B, Minko IG, Wood TG, Ceci JD, George S, Ballinger SW, Corless CL, McCullough AK, Lloyd RS. The metabolic syndrome resulting from a knockout of the NEIL1 DNA glycosylase. Proc Natl Acad Sci U S A. 2006; 103:1864–1869. [PubMed: 16446448]

42. Sampath H, Batra AK, Vartanian V, Carmical JR, Prusak D, King IB, Lowell B, Earley LF, Wood TG, Marks DL, McCullough AK, RSL. Variable penetrance of metabolic phenotypes and development of high-fat diet-induced adiposity in NEIL1-deficient mice. Am J Physiol Endocrinol Metab. 2011; 300:E724–734. [PubMed: 21285402]

43. Anstey AV, Ryan A, Rhodes LE, Charman CR, Arlett CF, Tyrrell RM, Taylor CR, Pearse AD. Characterization of photosensitivity in the Smith-Lemli-Opitz syndrome: a new congenital photosensitivity syndrome. Br J Dermatol. 1999; 141:406–414. [PubMed: 10583043]

44. Charman CR, Ryan A, Tyrrell RM, Pearse AD, Arlett CF, Kurwa HA, Shortland G, Anstey A. Photosensitivity associated with the Smith-Lemli-Opitz syndrome. Br J Dermatol. 1998; 138:885–888. [PubMed: 9666840]

45. Schulenburg-Brand D, Katugampola R, Anstey AV, Badminton MN. The cutaneous porphyrias. Dermatol Clin. 2014; 32:369–384. ix. [PubMed: 24891059]

46. Besur S, Schmeltzer P, Bonkovsky HL. Acute Porphyrias. J Emerg Med. 2015; 49:305–312. [PubMed: 26159905]

47. Geldenhuys S, Hart PH, Endersby R, Jacoby P, Feelisch M, Weller RB, Matthews V, Gorman S. Ultraviolet radiation suppresses obesity and symptoms of metabolic syndrome independently of vitamin D in mice fed a high-fat diet. Diabetes. 2014; 63:3759–3769. [PubMed: 25342734]

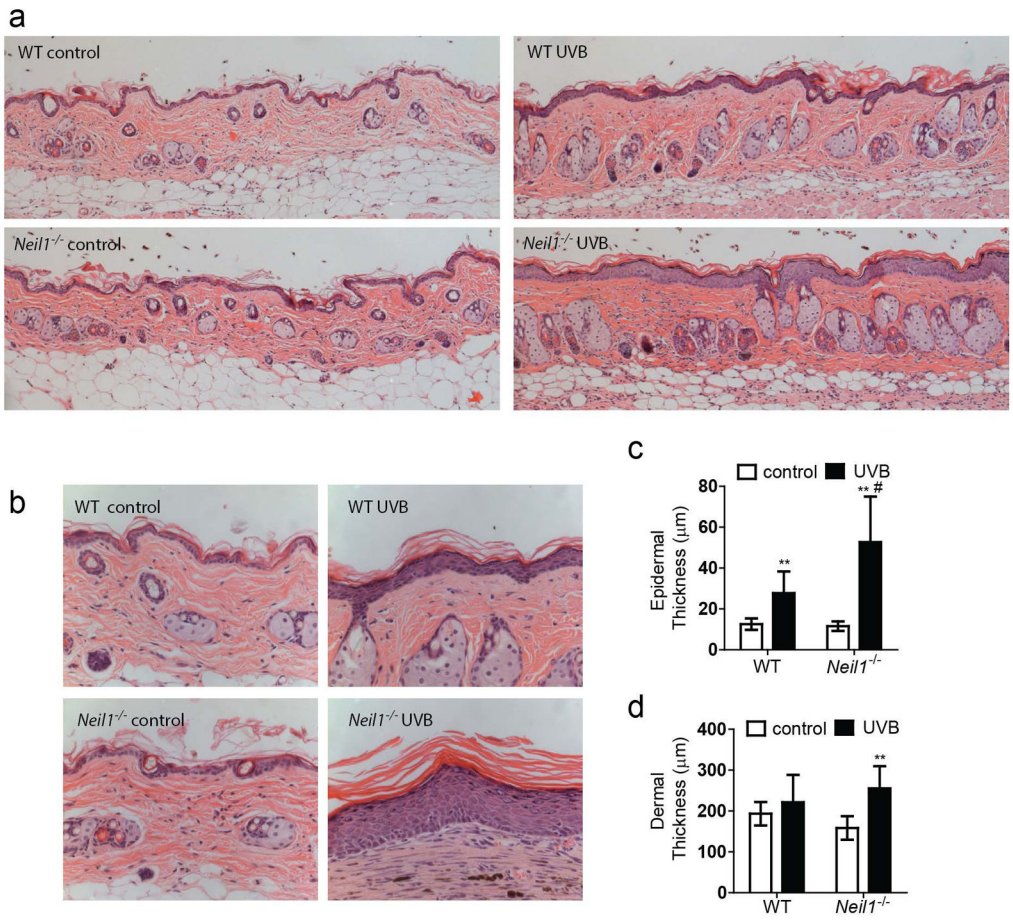

Fig. 1.

Chronic UVB exposure leads to characteristic skin morphology changes in WT and *Neil1*$^{-/-}$ mice. Dorsal skin was harvested from WT and *Neil1*$^{-/-}$ mice that were either not irradiated or exposed to chronic UVB and processed for histology. H&E stained sections were evaluated at 200x (Panel a) and 400x (Panel b) for characteristic morphological changes, including quantitative comparisons of epidermal thickness (Panel c) and dermal thickness (Panel d). Graphical data are presented as mean ± SD. WT un-irradiated, n = 5; WT irradiated, n = 20; *Neil1* $^{-/-}$ un-irradiated, n = 5; *Neil1* $^{-/-}$ irradiated, n = 17. ** $p < 0.01$ compared to WT un-irradiated, # $p < 0.05$ compared to WT UVB.

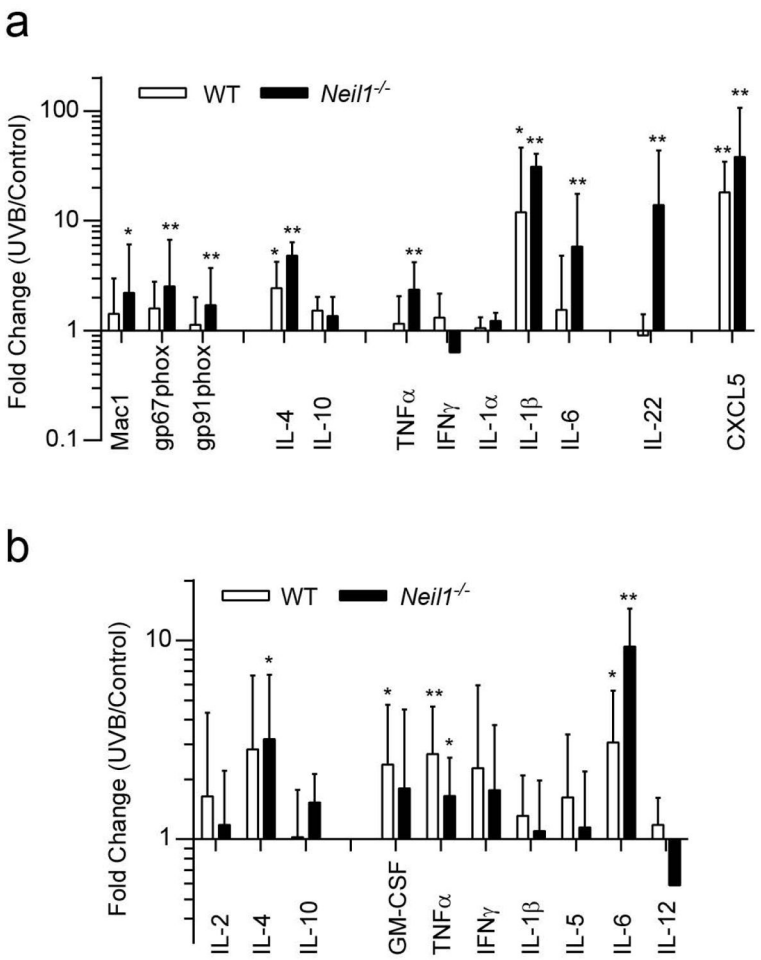

Fig. 2.

Increased inflammation markers following chronic UVB irradiation. Quantitative PCR were performed on dorsal skin tissue from un-irradiated and chronic UVB irradiated mice (Panel a) for markers of inflammation and UV response. Data are presented as mean ± SD. Errors for un-irradiated are not shown. WT un-irradiated, n = 6; WT irradiated, n = 8; *Neil1*$^{-/-}$ un-irradiated, n = 6; *Neil1*$^{-/-}$ irradiated, n = 8. Plasma levels of several cytokines (Panel b) were measured using a Luminex cytokine panel. Data are presented as mean ± SD. Errors for un-irradiated are not shown. WT un-irradiated, n = 5; WT irradiated, n = 20; *Neil1*$^{-/-}$ un-irradiated, n = 5; *Neil1*$^{-/-}$ irradiated, n = 17. * $p < 0.05$ compared to un-irradiated, * $p < 0.05$ and ** $p < 0.01$ compared to un-irradiated of same genotype.

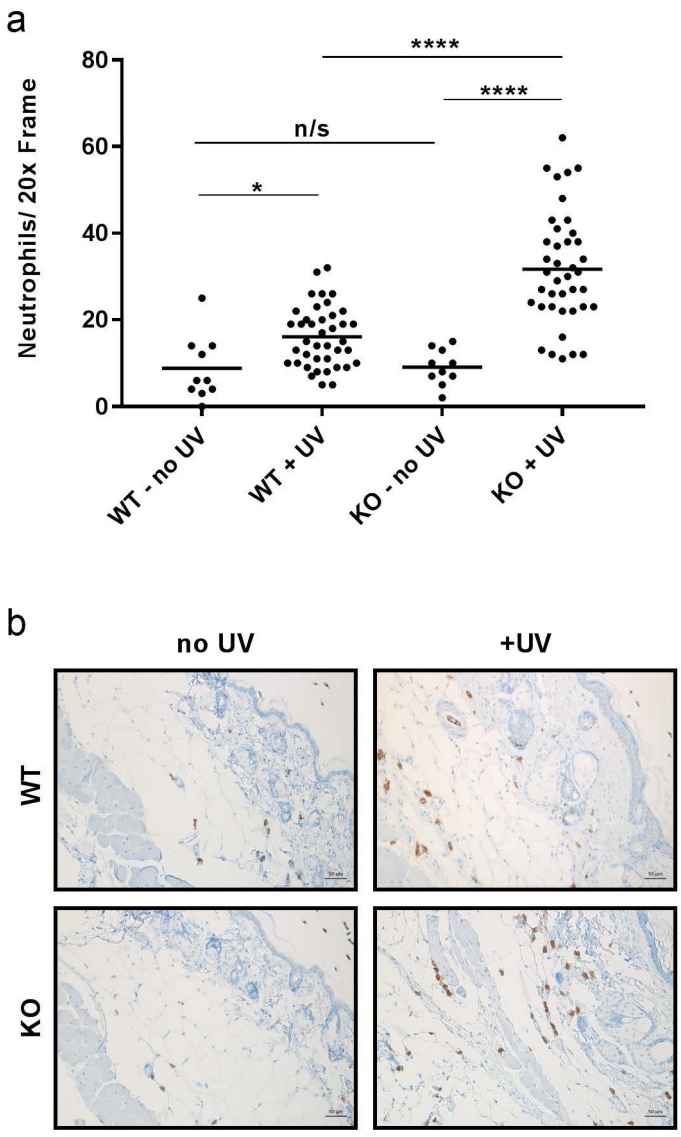

Fig. 3.

Enhanced neutrophil infiltration in *Neil1*$^{-/-}$ mice following UV exposure. a) Quantitation of neutrophils in un-irradiated and irradiated skin from WT and *Neil1*$^{-/-}$ mice as measured by Ly6C/Ly6G immunostaining. A total of 10 frames were scored for each of the no-UV samples; a total of 40 frames each were scored for the irradiated samples. Statistical analyses were done using Welches t-test (assuming non-equal SD) and follow standard denotation *<0.05, **<0.01, ***<0.001 and ****<0.0001. b) Representative images from (a) taken at 20x.

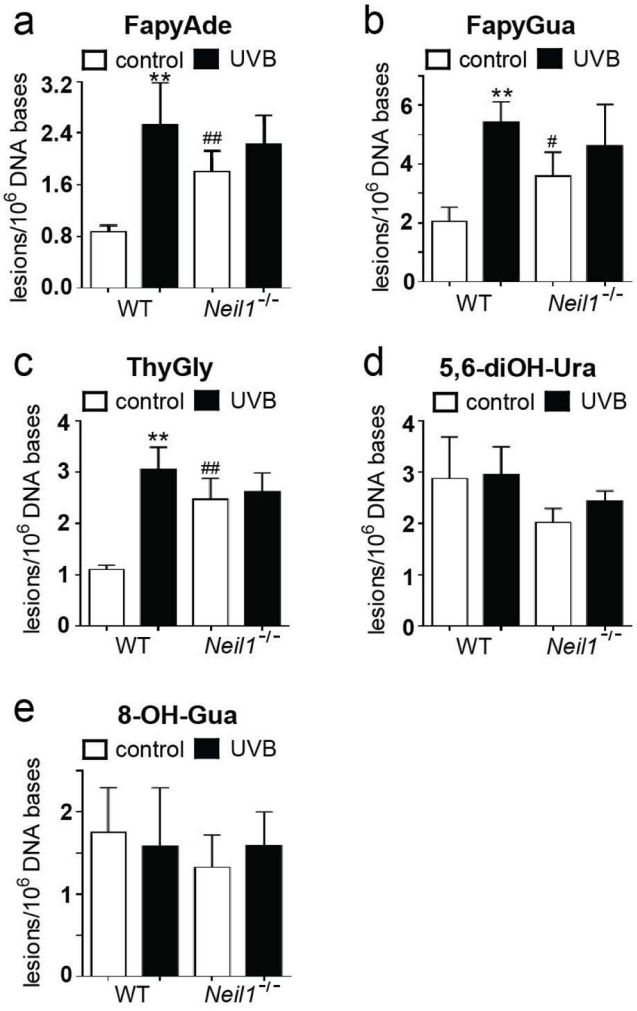

Fig. 4.

Steady-state ROS-induced DNA base damage increases in chronic UVB irradiated WT and in *Neil1*$^{-/-}$ mice. Levels of ROS-induced DNA base lesions were measured by GC-MS/MS. FapyAde (Panel a), FapyGua (Panel b), ThyGly (Panel c), 5,6-diOH-Ura (Panel d), and 8-OH-Gua (Panel e) were measured. Data are presented as mean ± SD. WT, n = 5; *Neil1*$^{-/-}$, n = 5; ** $p < 0.01$ compared to un-irradiated of same genotype. # $p < 0.05$ and ## $p < 0.01$ compared to WT.